



Transient Stress Wave Propagation in One-Dimensional Micropolar Bodies

by C. L. Randow and G. A. Gazonas

ARL-RP-238

February 2009

A reprint from the *International Journal of Solids and Structures*,
vol. 46, pp. 1218–1228, 2009.

NOTICES

Disclaimers

The findings in this report are not to be construed as an official Department of the Army position unless so designated by other authorized documents.

Citation of manufacturer's or trade names does not constitute an official endorsement or approval of the use thereof.

Destroy this report when it is no longer needed. Do not return it to the originator.

Army Research Laboratory

Aberdeen Proving Ground, MD 21005-5069

ARL-RP-238**February 2009**

Transient Stress Wave Propagation in One-Dimensional Micropolar Bodies

C. L. Randow and G. A. Gazonas
Weapons and Materials Research Directorate, ARL

A reprint from the *International Journal of Solids and Structures*,
vol. 46, pp. 1218–1228, 2009.

REPORT DOCUMENTATION PAGE				Form Approved OMB No. 0704-0188	
<p>Public reporting burden for this collection of information is estimated to average 1 hour per response, including the time for reviewing instructions, searching existing data sources, gathering and maintaining the data needed, and completing and reviewing the collection information. Send comments regarding this burden estimate or any other aspect of this collection of information, including suggestions for reducing the burden, to Department of Defense, Washington Headquarters Services, Directorate for Information Operations and Reports (0704-0188), 1215 Jefferson Davis Highway, Suite 1204, Arlington, VA 22202-4302. Respondents should be aware that notwithstanding any other provision of law, no person shall be subject to any penalty for failing to comply with a collection of information if it does not display a currently valid OMB control number.</p> <p>PLEASE DO NOT RETURN YOUR FORM TO THE ABOVE ADDRESS.</p>					
1. REPORT DATE (DD-MM-YYYY) February 2009		2. REPORT TYPE Reprint		3. DATES COVERED (From - To) January 2007–July 2008	
4. TITLE AND SUBTITLE Transient Stress Wave Propagation in One-Dimensional Micropolar Bodies				5a. CONTRACT NUMBER	
				5b. GRANT NUMBER	
				5c. PROGRAM ELEMENT NUMBER	
6. AUTHOR(S) C. L. Randow and G. A. Gazonas				5d. PROJECT NUMBER 62105AH84	
				5e. TASK NUMBER	
				5f. WORK UNIT NUMBER	
7. PERFORMING ORGANIZATION NAME(S) AND ADDRESS(ES) U.S. Army Research Laboratory ATTN: AMSRD-ARL-WM-MD Aberdeen Proving Ground, MD 21005-5069				8. PERFORMING ORGANIZATION REPORT NUMBER ARL-RP-238	
9. SPONSORING/MONITORING AGENCY NAME(S) AND ADDRESS(ES)				10. SPONSOR/MONITOR'S ACRONYM(S)	
				11. SPONSOR/MONITOR'S REPORT NUMBER(S)	
12. DISTRIBUTION/AVAILABILITY STATEMENT Approved for public release; distribution is unlimited.					
13. SUPPLEMENTARY NOTES A reprint from the <i>International Journal of Solids and Structures</i> , vol. 46, pp. 12181–1228, 2009.					
14. ABSTRACT Certain types of structures and materials, such as engineered multi-scale systems and comminuted zones in failed ceramics, may be modeled using continuum theories incorporating additional kinematic degrees of freedom beyond the scope of classical continuum theories. If such material systems are to be subjected to high strain rate loads, such as those resulting from ballistic impact or blast, it will be necessary to develop models capable of describing transient stress wave propagation through these media. Such a model is formulated, solved, and applied to the impact between two bodies and to a two-layer bar or strip subjected to an instantaneously applied stress. Results from these examples suggest that the model parameters, and therefore constitutive properties and geometries, may be tuned to reduce and control the transmission of stress through these bodies.					
15. SUBJECT TERMS wave propagation, micropolar media, impact, granular media					
16. SECURITY CLASSIFICATION OF:			17. LIMITATION OF ABSTRACT UL	18. NUMBER OF PAGES 22	19a. NAME OF RESPONSIBLE PERSON G. A. Gazonas
a. REPORT UNCLASSIFIED	b. ABSTRACT UNCLASSIFIED	c. THIS PAGE UNCLASSIFIED			19b. TELEPHONE NUMBER (Include area code) 410-306-0863



Transient stress wave propagation in one-dimensional micropolar bodies

C.L. Randow*, G.A. Gazonas

U.S. Army Research Laboratory, ATTN: AMSRD-ARL-WM-MD, Aberdeen Proving Ground, MD 21005-5069, USA

ARTICLE INFO

Article history:

Received 24 September 2007

Received in revised form 18 October 2008

Available online 30 October 2008

Keywords:

Microstructures

Stress waves

Plate impact

Anisotropic material

ABSTRACT

Certain types of structures and materials, such as engineered multi-scale systems and comminuted zones in failed ceramics, may be modeled using continuum theories incorporating additional kinematic degrees of freedom beyond the scope of classical continuum theories. If such material systems are to be subjected to high strain rate loads, such as those resulting from ballistic impact or blast, it will be necessary to develop models capable of describing transient stress wave propagation through these media. Such a model is formulated, solved, and applied to the impact between two bodies and to a two-layer bar or strip subjected to an instantaneously applied stress. Results from these examples suggest that the model parameters, and therefore constitutive properties and geometries, may be tuned to reduce and control the transmission of stress through these bodies.

Published by Elsevier Ltd.

1. Introduction

There is significant research interest in developing new materials and structures with improved survivability when subjected to high strain rate loadings associated with ballistic impact and/or blast. These new material systems may be created with sub-structures and components of different length scales, the combined effect of which is to better dissipate the energy of the blast or impact. Such multi-scale systems require more advanced models of the kind discussed in this work, which are often referred to as micropolar or Cosserat models, e.g. Mindlin (1964) and Eringen (1999). Models of this type possess additional kinematic degrees of freedom, e.g., a point in such a continuum may be capable of both translation and rotation. With additional degrees of freedom come additional constitutive properties and stress terms.

Improving our understanding of failure mechanisms and making use of this knowledge in developing improved predictive models is another aspect of ongoing research. For example, regions of armor-grade ceramics are often pulverized as a result of impact. The modeling of these post-failure comminution zones may be improved by viewing such zones as regions of granular media, another field of study where micropolar models allowing rotations of individual particles are often employed. Just as a cohesive zone has been used to model damage in an elastic strip by Gazonas and Allen (2003), so also a micropolar layer could be used to describe the failed region in a ceramic subjected to secondary impacts.

Various experiments have been developed to characterize material properties by subjecting test specimens to impact loads and measuring resulting deformations and propagating stress

waves, such as the split Hopkinson pressure bar and the plate impact test. The plate impact test, for example, effects a state of uniaxial strain well suited to a one-dimensional analysis. The analytical solutions to simplified, one-dimensional models may give insight into the behavior of materials subjected to such tests, suggest desirable constitutive properties or design parameters, and allow for the determination of constitutive properties from experimental results.

Although this work uses a one-dimensional, linear, anisotropic micropolar model to analyze the effect of instantaneously applied loads or impacts leading to transient wave propagation, there are many other works available in the literature that consider related problems. The governing equations developed in Section 2 are similar to those encountered in the study of helical springs by Jiang et al. (1991) and twisted ropes or cables by Samras et al. (1974), Ostoja-Starzewski (2002), and Shahsavari and Ostoja-Starzewski (2005), namely a system of two coupled partial differential equations (PDEs). Raoof et al. (1994) modeled an impact by applying a step load to a spiral strand. In much of the literature, harmonic solutions are considered in the study of wave propagation in micropolar media. For example, harmonic solutions were obtained for wave propagation along a composite wire rope using coupled PDEs by Martin and Berger (2002) similar to those used in the present work. Krishnaswamy and Batra (1998) examined wave propagation in a linear, infinite Cosserat rod with two directors and examined the effects of dispersion while considering harmonic motion. Finally, although the majority of the literature considers the linear problem, there has been some recent work studying wave propagation in non-linear systems by Porubov and Pastrone (2004) and Pastrone (2005).

A more general consequence of the coupled PDEs used in the present work is the existence of multiple waves. Applying a stress

* Corresponding author. Tel.: +1 410 306 1007; fax: +1 410 306 0806.

E-mail address: charles.randow@arl.army.mil (C.L. Randow).

pulse at one end of a one-dimensional micropolar bar will lead to two axial stress waves with different wave speeds traveling down the bar. Some other examples from physics of this phenomenon include birefringence (the decomposition of a single ray of light into two waves) and wave propagation in poroelastic columns, see Schanz and Cheng (2000, 2001). This latter example results in a system of two coupled PDEs for the one-dimensional case in terms of displacement and pore pressure based on Biot's theory of poroelasticity. Two compressional waves were then observed in the resulting one-dimensional model of a poroelastic column. Plona (1980) also makes reference to Biot's theory when he discusses his experimental observations of a second compressional wave in a porous medium. It is hoped that the work presented in this paper may benefit applications with similarly coupled systems of governing differential equations.

In Section 2 of this paper, the mixed initial-boundary value problem for two different micropolar systems is formulated. The first system is a two-layer bar rigidly fixed at one end with a stress applied at the other end. The second system consists of two different micropolar bodies, a flyer and a target, impacting one another. An equivalent discrete model of a rigidly fixed bar is included to provide additional physical insight by relating the model parameters from the continuum model to the discrete model. The solution methods used for these problems are described in Section 3 and include both a Laplace transform approach and a D'Alembert approach to solving the boundary value problems. Section 4 contains five different examples including: an analysis of a discrete system, a comparison between the discrete and the continuous systems, a number of impact examples, and a study on reflection and transmission coefficients due to impedance mismatch between different materials. Finally, Section 5 summarizes the results of this work and suggests some ways these results may be used and expanded upon in future studies.

2. Formulation of the governing equations

The general form of the mixed boundary-initial value problem describing the behavior of a linear, one-dimensional, anisotropic, micropolar body is presented in Section 2.1. Two particular configurations, a two-layer bar and an impact problem, are formulated in Sections 2.2 and 2.3. Finally, details of an equivalent discrete model are presented in Section 2.4. Although the main emphasis is the analysis of continuous problems, the discrete problem is included to provide additional physical insight into the nature of micropolar media.

2.1. Micropolar continuum model

The balance of linear momentum and the balance of angular momentum equations for a micropolar body are given by Eringen (1999) as follows:

$$\{\mathbf{T}\}_{kl,k} = \rho \frac{\partial^2}{\partial t^2} \{\mathbf{u}\}_l, \quad \{\mathbf{M}\}_{kl,k} + \epsilon_{lkm} \{\mathbf{T}\}_{km} = \rho j_{lk} \frac{\partial^2}{\partial t^2} \{\boldsymbol{\varphi}\}_k, \quad (2.1)$$

where the second-order tensors \mathbf{T} and \mathbf{M} and the vectors \mathbf{u} and $\boldsymbol{\varphi}$ are defined over $\mathbf{x} \in \overline{\mathcal{V}}$, $t \in T^+$. The micropolar body occupies the region $\overline{\mathcal{V}}$ in Euclidean space; time T^+ is defined over the range $[0, \infty)$. For a micropolar body, there are two stress tensors: the (force) stress tensor \mathbf{T} and the couple stress tensor \mathbf{M} . In addition, there are two vectors describing the deformations of a micropolar body: the displacement vector \mathbf{u} and the microdisplacement vector $\boldsymbol{\varphi}$. The mass density ρ and the microinertia j_{lk} also appear in Eq. (2.1). Standard indicial notation is used, i.e., $\{\mathbf{u}\}_l$ denotes the l th component of the vector \mathbf{u} , the notation $_{,k}$ denotes the partial derivative with respect to position, and ϵ_{lkm} is the permutation symbol. Note that there are no body force or body couple terms included in Eq. (2.1).

For the one-dimensional model under consideration, the position along the body's length is parameterized by x . The strain measures for the normal strain, ε , and the micropolar strain, γ , are

$$\varepsilon = \frac{\partial u}{\partial x}, \quad \gamma = \frac{\partial \varphi}{\partial x}. \quad (2.2)$$

As is often done in micropolar models, φ is considered to be a rotation and u is an axial deformation¹ as shown in Fig. 1. The constitutive relations for the one-dimensional, elastic, anisotropic, micropolar system considered in this work are given by

$$\{\mathbf{T}\}_{11} = T = \tilde{A}\varepsilon + \tilde{C}\gamma, \quad \{\mathbf{M}\}_{11} = M = \tilde{C}\varepsilon + \tilde{B}\gamma. \quad (2.3)$$

The constitutive parameters \tilde{A} , \tilde{B} , and \tilde{C} describe the elastic behavior of the model and control the coupling, or interaction, between the two kinematic modes: extension and rotation, see the terms C_1 – C_4 in Shahsavari and Ostoja-Starzewski (2005). (The tilde over the model parameters indicates that these are dimensional quantities; non-dimensional parameters will be introduced shortly.) Applying Eqs. (2.2) and (2.3) to Eq. (2.1) leads to the following system of PDEs:

$$\tilde{A} \frac{\partial^2 u}{\partial x^2} + \tilde{C} \frac{\partial^2 \varphi}{\partial x^2} = \rho \frac{\partial^2 u}{\partial t^2}, \quad \tilde{C} \frac{\partial^2 u}{\partial x^2} + \tilde{B} \frac{\partial^2 \varphi}{\partial x^2} = \rho j \frac{\partial^2 \varphi}{\partial t^2}, \quad (2.4)$$

where for a one-dimensional system the microinertia term j_{lk} from Eq. (2.1) becomes the scalar j . Eq. (2.4) are second-order, linear PDEs that require two initial conditions and two boundary conditions for each kinematic quantity, u and φ . Eq. (2.4) may be written in the following non-dimensional form:

$$A \nabla^2 u + C \nabla^2 \varphi = \ddot{u}, \quad C \nabla^2 u + B \nabla^2 \varphi = D \ddot{\varphi}, \quad (2.5)$$

where

$$A = \frac{\tilde{A}\tau^2}{\rho\delta^2}, \quad B = \frac{\tilde{B}\tau^2}{\rho\delta^4}, \quad C = \frac{\tilde{C}\tau^2}{\rho\delta^3}, \quad D = \frac{j}{\delta^2}. \quad (2.6)$$

The terms A , B , C , and D are non-dimensional; τ is unit time and δ is unit length. In addition, the derivatives indicated by ∇ and the dots are now derivatives with respect to position normalized by δ and time normalized by τ , respectively; x and t will now be taken as non-dimensional quantities normalized by δ and τ .

One form of the strain energy density that yields the desired system of governing equations following Hamilton's principle is given by

$$W = \frac{\rho\delta^2}{\tau^2} \frac{1}{2} [A(\nabla u)^2 + 2C\nabla u \nabla \varphi + B(\nabla \varphi)^2], \quad (2.7)$$

such that the (force) stress and the couple stress are equivalent to Eq. (2.3) and are given by

$$T = \frac{\partial W}{\partial \varepsilon} = \frac{\rho\delta^2}{\tau^2} (A\nabla u + C\nabla \varphi), \quad M = \frac{\partial W}{\partial \gamma} = \frac{\rho\delta^3}{\tau^2} (C\nabla u + B\nabla \varphi). \quad (2.8)$$

To ensure stability of the thermodynamic state of the system, it is necessary for $W \geq 0$ for all possible applied normalized strains ∇u and $\nabla \varphi$, see Eringen (1999). The following inequalities are consequences of this requirement:

$$A > 0, \quad B > 0, \quad AB - C^2 > 0. \quad (2.9)$$

The boundary conditions to be applied to Eq. (2.5) may include both

¹ For the one-dimensional case, there is no distinction in the governing equations for different orientations of rotational motion, since $j_{lk} = 0$ for $l \neq k$ and $j_{ll} \neq 0$ for only a single value of l . There will always be two governing differential equations of the form of Eq. (2.4) based on two constitutive relations of the form of Eq. (2.3), although the subscripts may differ.

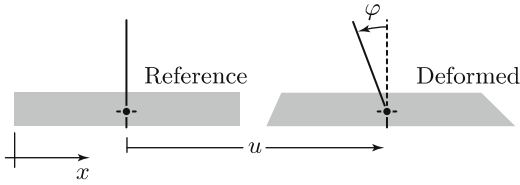


Fig. 1. Owing kinematic quantities u and φ by tracking a point from its reference configuration to a deformed configuration.

essential and natural conditions. For example, if \hat{u} and $\hat{\varphi}$ represent the normalized deformation and rotation at a boundary and if \hat{T} and \hat{M} represent the normalized (force) stress and couple stress at a boundary, then the essential boundary conditions consist of

$$u|_{x=0,1} = \hat{u}, \quad \varphi|_{x=0,1} = \hat{\varphi}, \quad t \in [0, \infty), \quad (2.10)$$

while the natural boundary conditions consist of

$$A \nabla u|_{x=0,1} + C \nabla \varphi|_{x=0,1} = \hat{T}, \quad C \nabla u|_{x=0,1} + B \nabla \varphi|_{x=0,1} = \hat{M}, \quad t \in [0, \infty), \quad (2.11)$$

recalling Eq. (2.8). The non-dimensional stress terms \hat{T} and \hat{M} are obtained by normalizing by $\rho \delta^2 \tau^{-2}$ and $\rho \delta^3 \tau^{-2}$, respectively. Initial conditions specify the initial velocities in terms of both kinematic quantities, \dot{u} and $\dot{\varphi}$. In other words

$$\dot{u}|_{t=0} = \hat{v}, \quad \dot{\varphi}|_{t=0} = \hat{\omega}, \quad x \in [0, 1], \quad (2.12)$$

where \hat{v} is the normalized initial axial velocity and $\hat{\omega}$ is the normalized initial rotational velocity. In addition, it is assumed that at time $t = 0$ the body is stress-free, recall Eq. (2.8), i.e.

$$A \nabla u|_{t=0} + C \nabla \varphi|_{t=0} = 0, \quad C \nabla u|_{t=0} + B \nabla \varphi|_{t=0} = 0, \quad x \in [0, 1]. \quad (2.13)$$

It is apparent that C controls the coupling between the translation and rotation; it will be shown that A is related to the elastic modulus for the classical, non-polar case.

2.2. Boundary and initial conditions for the two-layer problem

Consider the bar consisting of two different micropolar layers, layer 1 and layer 2, rigidly fixed at $x = 1$ as shown in Fig. 2. The properties for layer 1 are given by A_1 , B_1 , C_1 , and D_1 ; for layer 2, these properties are given by A_2 , B_2 , C_2 , and D_2 . If the first body is of length l , where $0 < l < 1$, and the second body is of length $1 - l$, it follows from Eq. (2.5) that the governing equations for the two bodies are

$$A_1 \nabla^2 u_1 + C_1 \nabla^2 \varphi_1 = \ddot{u}_1, \quad C_1 \nabla^2 u_1 + B_1 \nabla^2 \varphi_1 = D_1 \ddot{\varphi}_1, \quad (2.14)$$

$$A_2 \nabla^2 u_2 + C_2 \nabla^2 \varphi_2 = \ddot{u}_2, \quad C_2 \nabla^2 u_2 + B_2 \nabla^2 \varphi_2 = D_2 \ddot{\varphi}_2, \quad (2.15)$$

where u_1 and φ_1 are defined over the range $x \in [0, l]$ and u_2 and φ_2 are defined over the range $x \in [l, 1]$. Recalling Eqs. (2.12) and (2.13), the initial conditions for a stationary body with zero stress state are given by

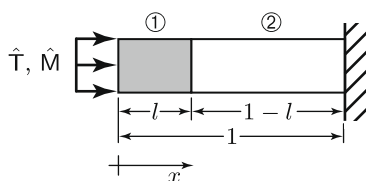


Fig. 2. A body consisting of two different micropolar layers is subjected to a known normalized (force) stress and couple stress at $x = 0$ and is rigidly fixed at $x = 1$.

$$\dot{u}_1|_{t=0} = \dot{u}_2|_{t=0} = 0, \quad \dot{\varphi}_1|_{t=0} = \dot{\varphi}_2|_{t=0} = 0, \quad (2.16)$$

and

$$A_1 \nabla u_1|_{t=0} + C_1 \nabla \varphi_1|_{t=0} = 0, \quad C_1 \nabla u_1|_{t=0} + B_1 \nabla \varphi_1|_{t=0} = 0, \quad (2.17)$$

$$A_2 \nabla u_2|_{t=0} + C_2 \nabla \varphi_2|_{t=0} = 0, \quad C_2 \nabla u_2|_{t=0} + B_2 \nabla \varphi_2|_{t=0} = 0. \quad (2.18)$$

Instead of using Eqs. (2.17) and (2.18), but consistent with those equations, we will assume that the bodies are initially undeformed, i.e.

$$u_1|_{t=0} = u_2|_{t=0} = 0, \quad \varphi_1|_{t=0} = \varphi_2|_{t=0} = 0. \quad (2.19)$$

The essential boundary conditions at $x = 1$ are given by

$$u_2|_{x=1} = 0, \quad \varphi_2|_{x=1} = 0, \quad (2.20)$$

while the natural boundary conditions at $x = 0$ are given by

$$A_1 \nabla u_1|_{x=0} + C_1 \nabla \varphi_1|_{x=0} = \hat{T}, \quad C_1 \nabla u_1|_{x=0} + B_1 \nabla \varphi_1|_{x=0} = \hat{M}, \quad (2.21)$$

recalling Eqs. (2.10) and (2.11). Finally, the matching boundary conditions at the interface $x = l$ are given by

$$u_1|_{x=l} = u_2|_{x=l}, \quad (2.22)$$

$$\varphi_1|_{x=l} = \varphi_2|_{x=l}, \quad (2.23)$$

$$A_1 \nabla u_1|_{x=l} + C_1 \nabla \varphi_1|_{x=l} = A_2 \nabla u_2|_{x=l} + C_2 \nabla \varphi_2|_{x=l}, \quad (2.24)$$

$$C_1 \nabla u_1|_{x=l} + B_1 \nabla \varphi_1|_{x=l} = C_2 \nabla u_2|_{x=l} + B_2 \nabla \varphi_2|_{x=l}, \quad (2.25)$$

for $t \in [0, \infty)$. The complete mixed boundary-initial value problem is given by Eqs. (2.14)–(2.16), (2.20)–(2.25).

2.3. Boundary and initial conditions for the impact problem

Consider now the impact between two micropolar bodies, as shown in Fig. 3. This problem is similar to that presented in Section 2.2 in that there are two different bodies with two sets of material properties given by the constants A_1 , B_1 , C_1 , and D_1 for the initially moving body (the flyer) and A_2 , B_2 , C_2 , and D_2 for the initially stationary body (the target). The governing equations are given by Eqs. (2.14) and (2.15).

The first body is traveling at an initial normalized velocity \hat{v} and, at $t = 0$, it impacts the target. Therefore, the initial conditions must specify both the initial velocities as in YuFeng and DeChao (1998) and Goldsmith (1999):

$$\dot{u}_1|_{t=0} = \hat{v}_1 = \hat{v}, \quad \dot{\varphi}_1|_{t=0} = \hat{\omega}_1 = 0, \quad (2.26)$$

$$\dot{u}_2|_{t=0} = \hat{v}_2 = 0, \quad \dot{\varphi}_2|_{t=0} = \hat{\omega}_2 = 0, \quad (2.27)$$

as well as the initial undeformed state, which is described by Eq. (2.19). As shown in Fig. 3, the free ends of both bodies ($x = 0$ and $x = 1$) are stress-free leading to the boundary conditions

$$A_1 \nabla u_1|_{x=0} + C_1 \nabla \varphi_1|_{x=0} = 0, \quad C_1 \nabla u_1|_{x=0} + B_1 \nabla \varphi_1|_{x=0} = 0, \quad (2.28)$$

$$A_2 \nabla u_2|_{x=1} + C_2 \nabla \varphi_2|_{x=1} = 0, \quad C_2 \nabla u_2|_{x=1} + B_2 \nabla \varphi_2|_{x=1} = 0. \quad (2.29)$$

The matching conditions at $x = l$ are identical to those given by Eqs. (2.22)–(2.24) and (2.25). The mixed boundary-initial value problem

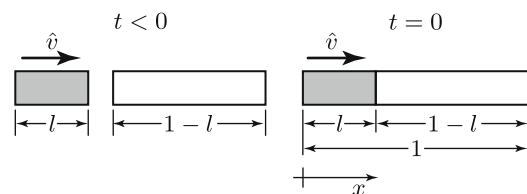


Fig. 3. Two micropolar bodies are shown before impact ($t < 0$) and at the moment of impact ($t = 0$). The first body of length l (the flyer) is traveling with a normalized velocity \hat{v} ; the second body of length $1 - l$ (the target) is initially at rest.

is thus given by Eqs. (2.14), (2.15), (2.19), (and), (2.23)–(2.27) 2.28 (and 2.29).

2.4. The discrete model

Although the primary goal of the present work is to study continuous problems, a brief outline of an *equivalent* discrete system may be helpful to provide some physical interpretation of the results. A discrete system consisting of a series of masses and connecting springs is shown in Fig. 4. This model is similar to that introduced in the study of dynamic behavior of granular media by Lisina et al. (2001) and Pavlov et al. (2006). Each mass is connected to each neighbor with two springs: one spring with spring constant k_0 connects the centers of each mass and one spring with spring constant k_1 connects the corners of each mass. A given mass i is allowed to translate horizontally (u_i) and rotate in the plane of the page about its center (φ_i). In future work, it may be interesting to consider non-linear springs, e.g., non-monotone springs as in Balk et al. (2001) or bi-stable springs as in Puglisi and Truskinovsky (2000) or Slepian et al. (2005).

For a system with n masses, the total energy of the system is found by summing the energy associated with the deformation of each spring:

$$U = \sum_{i=1}^{n-1} \frac{1}{2} k_0 (u_{i+1} - u_i)^2 + \frac{1}{2} k_1 [u_{i+1} - u_i + a(\varphi_i - \varphi_{i+1})]^2, \quad (2.30)$$

where only linear terms are retained from the development of the equations based on Fig. 4. The $2n$ Lagrange's equations are obtained by taking derivatives of U with respect to the n discrete axial displacements and the n discrete rotations corresponding to each of the n masses.

In addition to obtaining a system of Lagrange's equations, by applying a Taylor series expansion of the displacement terms we may also obtain the continuum version of the discrete model in the following form:

$$[l^2(k_0 + k_1)] \frac{\partial^2 u}{\partial x^2} + (-al^2 k_1) \frac{\partial^2 \varphi}{\partial x^2} = m \frac{\partial^2 u}{\partial t^2}, \quad (2.31)$$

$$(-al^2 k_1) \frac{\partial^2 u}{\partial x^2} + (a^2 l^2 k_1) \frac{\partial^2 \varphi}{\partial x^2} = I \frac{\partial^2 \varphi}{\partial t^2}, \quad (2.32)$$

where m and I refer to the mass and the mass moment of inertia of each mass in the system. Comparing Eqs. (2.31) and (2.32) with (2.4), it follows that the constitutive parameters from the continuum case may be related to the discrete parameters as follows:

$$\tilde{A} = l^2(k_0 + k_1)/V, \tilde{B} = a^2 l^2 k_1/V, \tilde{C} = -al^2 k_1/V, \rho = m/V, j = I/m, \quad (2.33)$$

where V is the volume of the continuum system obtained from the discrete system. Since $k_0, k_1, a, l, V > 0$, the inequalities from Eq. (2.9) are identically satisfied by Eq. (2.33).

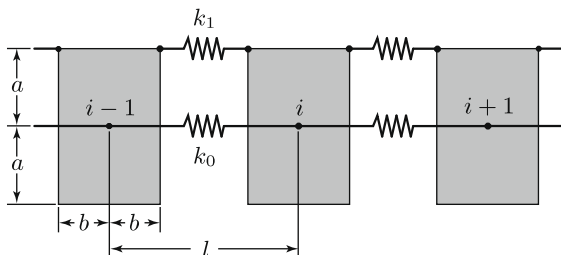


Fig. 4. Three discrete masses, $i-1$, i , and $i+1$, each allowed to translate axially and rotate about the mass center, are shown. One spring (k_0) connects the centers of adjacent masses together and another spring (k_1) connects opposing corners of adjacent masses.

3. Solving the boundary value problems and the discrete problem

In this section, three different solution techniques are described for the different problems presented in Section 2. In Section 3.1, the D'Alembert method is used to solve the bar problem described in Section 2.2. This approach is particularly useful in obtaining ratios of incident, reflected, and transmitted stress waves (reflection and transmission coefficients) across interfaces separating materials with different impedance values. A Laplace transform solution is described for the impact problem in Section 3.2 and a brief description of the solution method for the discrete problem of Section 2.4 is included in Section 3.3.

3.1. Solving the two-layer problem via the method of D'Alembert

One approach that may be used to solve the boundary value problem from Section 2.2 is to use a D'Alembert formulation. Recalling Fig. 2, solutions for Eqs. (2.14) and (2.15) for the case where both layers in a bar begin at rest are assumed to be of the form

$$u_1(x, t) = \mu_1 [F_1(t/\lambda_1^- + x) + F_2(t/\lambda_1^- - x)] + \mu_2 [F_3(t/\lambda_1^+ + x) + F_4(t/\lambda_1^+ - x)], \quad (3.1)$$

$$\varphi_1(x, t) = F_1(t/\lambda_1^- + x) + F_2(t/\lambda_1^- - x) + F_3(t/\lambda_1^+ + x) + F_4(t/\lambda_1^+ - x), \quad (3.2)$$

$$u_2(x, t) = \mu_3 [F_5(t/\lambda_2^- + x) + F_6(t/\lambda_2^- - x)] + \mu_4 [F_7(t/\lambda_2^+ + x) + F_8(t/\lambda_2^+ - x)], \quad (3.3)$$

$$\varphi_2(x, t) = F_5(t/\lambda_2^- + x) + F_6(t/\lambda_2^- - x) + F_7(t/\lambda_2^+ + x) + F_8(t/\lambda_2^+ - x). \quad (3.4)$$

The following constants are used in writing Eqs. (3.1)–(3.4):

$$\mu_1 = \frac{(\lambda_1^-)^2 - d_4}{d_3}, \mu_2 = \frac{(\lambda_1^+)^2 - d_4}{d_3}, \mu_3 = \frac{(\lambda_2^-)^2 - d_8}{d_7}, \mu_4 = \frac{(\lambda_2^+)^2 - d_8}{d_7}, \quad (3.5)$$

where

$$\lambda_1^\pm = \sqrt{d_1 + d_4 \pm \sqrt{d_1^2 + 4d_2d_3 - 2d_1d_4 + d_4^2}/\sqrt{2}}, \quad (3.6)$$

$$\lambda_2^\pm = \sqrt{d_5 + d_8 \pm \sqrt{d_5^2 + 4d_6d_7 - 2d_5d_8 + d_8^2}/\sqrt{2}}, \quad (3.7)$$

and the constants d_1, d_2, \dots, d_8 are functions of the model parameters as follows:

$$d_1 = \frac{B_1}{A_1B_1 - C_1^2}, \quad d_2 = \frac{-C_1D_1}{A_1B_1 - C_1^2}, \quad d_3 = \frac{-C_1}{A_1B_1 - C_1^2}, \quad (3.8)$$

$$d_4 = \frac{A_1D_1}{A_1B_1 - C_1^2}, \quad d_5 = \frac{B_2}{A_2B_2 - C_2^2}, \quad d_6 = \frac{-C_2D_2}{A_2B_2 - C_2^2}, \quad (3.9)$$

$$d_7 = \frac{-C_2}{A_2B_2 - C_2^2}, \quad d_8 = \frac{A_2D_2}{A_2B_2 - C_2^2}. \quad (3.10)$$

Based on the forms of Eqs. (3.6) and (3.7), it follows that $\lambda_1^+ > \lambda_1^-$ and $\lambda_2^+ > \lambda_2^-$. All eigenvalues are real as a consequence of the inequalities given by Eq. (2.9). The normalized velocities of the fast waves are $1/\lambda_1^-$ and $1/\lambda_2^-$ and the normalized velocities of the slow waves are $1/\lambda_1^+$ and $1/\lambda_2^+$. The ratios of the fast wave speeds to the slow wave speeds are thus λ_1^+/λ_1^- and λ_2^+/λ_2^- . This ratio will be designated Γ in the appendix, see Eq. (A.1).

For a non-polar material, there is infinite rotational stiffness so that there can be no rotation, i.e., $B \rightarrow \infty$. In this situation,

$1/\lambda^- \rightarrow 0$ and $1/\lambda^+ \rightarrow \sqrt{A}$. To write the wave speed in dimensional form, it is necessary to multiply by δ/τ , which is unit length per unit time. Recalling the first of Eq. (2.6), we see that

$$\sqrt{A}\left(\frac{\delta}{\tau}\right) = \sqrt{\frac{\tilde{A}\tau^2}{\rho\delta^2}}\left(\frac{\delta}{\tau}\right) = \sqrt{\frac{\tilde{A}}{\rho}} \Rightarrow \sqrt{\frac{E}{\rho}}, \quad (3.11)$$

where E is the elastic modulus, ρ is the mass density, and $\sqrt{E/\rho}$ is the classical wave speed for a one-dimensional elastic body. This shows that in the non-polar case, \tilde{A} corresponds to E .

We will now consider a simpler case with identical materials, i.e., the bar is homogeneous and there is no need for model parameter subscripts. It is then only necessary to solve for $u(x, t)$ and $\varphi(x, t)$ with stress applied at $x = 0$ and the bar rigidly fixed at $x = 1$. The next step is to use the definition of (force) stress and couple stress, Eq. (2.8), with the D'Alembert form of the displacement functions and the boundary conditions Eqs. (2.21) and (2.20) to obtain

$$(C + \mu_1 A) \nabla F_1(t/\lambda^-) - (C + \mu_1 A) \nabla F_2(t/\lambda^-) + (C + \mu_2 A) \nabla F_3(t/\lambda^+) - (C + \mu_2 A) \nabla F_4(t/\lambda^+) = \hat{T}, \quad (3.12)$$

$$(B + \mu_1 C) \nabla F_1(t/\lambda^-) - (B + \mu_1 C) \nabla F_2(t/\lambda^-) + (B + \mu_2 C) \nabla F_3(t/\lambda^+) - (B + \mu_2 C) \nabla F_4(t/\lambda^+) = \hat{M}, \quad (3.13)$$

$$\mu_1 F_1(t/\lambda^- + 1) + \mu_1 F_2(t/\lambda^- - 1) + \mu_2 F_3(t/\lambda^+ + 1) + \mu_2 F_4(t/\lambda^+ - 1) = 0, \quad (3.14)$$

$$F_1(t/\lambda^- + 1) + F_2(t/\lambda^- - 1) + F_3(t/\lambda^+ + 1) + F_4(t/\lambda^+ - 1) = 0. \quad (3.15)$$

After taking the Laplace transform of Eqs. 3.12, 3.13, 3.14, and 3.15, we may solve for the functions F_1 – F_4 to obtain

$$F_1 = \kappa_1 \sum_{n=0}^{\infty} \{(2 + 4n - x - t/\lambda^-) H[-2 - 4n + x + t/\lambda^-] + (-4 - 4n + x + t/\lambda^-) H[-4 - 4n + x + t/\lambda^-]\}, \quad (3.16)$$

$$F_2 = \kappa_1 \sum_{n=0}^{\infty} \{(2 + 4n + x - t/\lambda^-) H[-2 - 4n - x + t/\lambda^-] + (-4n - x + t/\lambda^-) H[-4n - x + t/\lambda^-]\}, \quad (3.17)$$

$$F_3 = \kappa_2 \sum_{n=0}^{\infty} \{(2 + 4n - x - t/\lambda^+) H[-2 - 4n + x + t/\lambda^+] + (-4 - 4n + x + t/\lambda^+) H[-4 - 4n + x + t/\lambda^+]\}, \quad (3.18)$$

$$F_4 = \kappa_2 \sum_{n=0}^{\infty} \{(2 + 4n + x - t/\lambda^+) H[-2 - 4n - x + t/\lambda^+] + (-4n - x + t/\lambda^+) H[-4n - x + t/\lambda^+]\}, \quad (3.19)$$

where

$$\kappa_1 = \frac{A_1 \mu_2 \hat{M} - B_1 \hat{T} + C_1 (\hat{M} - \mu_2 \hat{T})}{(\mu_1 - \mu_2)(A_1 B_1 - C_1^2)}, \quad (3.20)$$

$$\kappa_2 = -\frac{A_1 \mu_1 \hat{M} - B_1 \hat{T} + C_1 (\hat{M} - \mu_1 \hat{T})}{(\mu_1 - \mu_2)(A_1 B_1 - C_1^2)}, \quad (3.21)$$

and $H[\cdot]$ designates the Heaviside unit step function. The D'Alembert form of the solution will be used in Section 4.5 to obtain ratios of incident, reflected, and transmitted stress through an interface between materials with an impedance mismatch. Although the summations in Eqs. (3.16)–(3.18) and (3.19) are infinite, when a finite time t is considered, it is only necessary to include a finite number of terms in the summation due to the presence of the Heaviside functions.

3.2. Solving the impact problem via the Laplace transform

Laplace transforms will be used to solve the mixed boundary-initial value problems from Sections 2.2 and 2.3, although the impact example from Section 2.3 will be used to demonstrate the method. After taking the transforms of Eqs. (2.14) and (2.15) and applying the initial conditions as given by Eqs. 2.19, 2.26, and 2.27, we obtain the following ordinary differential equations:

$$A_1 \nabla^2 \bar{u}_1 + C_1 \nabla^2 \bar{\varphi}_1 = s^2 \bar{u}_1 - \hat{v}, \quad C_1 \nabla^2 \bar{u}_1 + B_1 \nabla^2 \bar{\varphi}_1 = D_1 s^2 \bar{\varphi}_1, \quad (3.22)$$

$$A_2 \nabla^2 \bar{u}_2 + C_2 \nabla^2 \bar{\varphi}_2 = s^2 \bar{u}_2, \quad C_2 \nabla^2 \bar{u}_2 + B_2 \nabla^2 \bar{\varphi}_2 = D_2 s^2 \bar{\varphi}_2, \quad (3.23)$$

where the bar indicates transformed functions and s is the variable in the Laplace domain. The general forms of the solutions to Eqs. (3.22) and (3.23) are

$$\bar{u}_1 = c_1 \mu_1 e^{-s \lambda_1^- x} + c_2 \mu_1 e^{s \lambda_1^- x} + c_3 \mu_2 e^{-s \lambda_1^+ x} + c_4 \mu_2 e^{s \lambda_1^+ x} + \hat{v}/s^2, \quad (3.24)$$

$$\bar{\varphi}_1 = c_1 e^{-s \lambda_1^- x} + c_2 e^{s \lambda_1^- x} + c_3 e^{-s \lambda_1^+ x} + c_4 e^{s \lambda_1^+ x}, \quad (3.25)$$

$$\bar{u}_2 = c_5 \mu_3 e^{-s \lambda_2^- x} + c_6 \mu_3 e^{s \lambda_2^- x} + c_7 \mu_4 e^{-s \lambda_2^+ x} + c_8 \mu_4 e^{s \lambda_2^+ x}, \quad (3.26)$$

$$\bar{\varphi}_2 = c_5 e^{-s \lambda_2^- x} + c_6 e^{s \lambda_2^- x} + c_7 e^{-s \lambda_2^+ x} + c_8 e^{s \lambda_2^+ x}, \quad (3.27)$$

where the eigenvalues and constants shown are defined by Eqs. (3.5)–(3.9) and (3.10). The eight constants c_1, \dots, c_8 are found by applying the general solutions given by Eqs. (3.24)–(3.26) and (3.27) to the eight boundary conditions given by Eqs. (2.22)–(2.24), (2.28), and (2.29). One consequence of applying these boundary conditions is that

$$c_1 = c_2, \quad c_3 = c_4, \quad c_5 = e^{2s \lambda_2^-} c_6, \quad c_7 = e^{2s \lambda_2^+} c_8. \quad (3.28)$$

At this point it is necessary to numerically invert the solutions from the Laplace domain to obtain the final solution in the time domain. The approach used in this work is the Dubner–Abate–Crump (DAC) algorithm described by Crump (1976); the effects of Gibbs phenomena in the solution will be reduced through the use of Lanczos's σ -factors, see Lavery and Gazonas (2006). Results from the Laplace transform solution are used in Sections 4.2, 4.3 and 4.4.

3.3. Solving the discrete problem

Using the commercial software package *Mathematica*, an explicit formulation is employed to solve the discrete problem. First, displacements u_i and φ_i are calculated by multiplying the longitudinal velocity v_i and rotational velocity ω_i by the time step Δt for each mass i . Accelerations are found by determining the net force and moment acting on each mass and dividing these terms by the mass m and mass moment of inertia I , respectively. The forces and moments acting on each mass are obtained from Eq. (2.30). The updated velocities v_i and ω_i are obtained by multiplying each acceleration by Δt . The process of finding displacements, accelerations, and velocities is repeated for each time step to obtain the dynamic response of the system. Results from the discrete model are used in Sections 4.1 and 4.2.

4. Results

In this section, five different examples will be considered that are based on the formulations and solutions discussed thus far. The first example in Section 4.1 shows a discrete model and it is used to illustrate the presence of two longitudinal waves. In Section 4.2, the discrete model is compared with an equivalent continuum model. An example of impact between two micropolar bodies with specially chosen model parameters is presented in Section 4.3. In Section 4.4, some additional impact examples are presented, including one that demonstrates the effect of impedance mismatch between target and flyer. Finally, the consequences of impedance mismatch are analyzed further in Section 4.5. In all plots shown,

time (the horizontal axis) has been normalized such that when normalized time equals one, the slow stress wave has travelled the length of the specimen. With the exception of Fig. 8, the vertical axes are normalized such that the overall length, the maximum velocity, or the maximum stress are set equal to one, depending on the results being plotted.

4.1. A discrete model

This example is the discrete equivalent to that described in Section 2.2. A discrete rod made up of 80 discrete masses ($n = 80$, see Fig. 4 and Eq. (2.30)) with one end rigidly fixed will be considered, i.e., $u_{80} = 0$ and $\varphi_{80} = 0$. At the free end, a constant compressive force of 0.1 N is instantaneously applied at time $t = 0$ s. In addition, the following model parameters have been chosen: $a = 19.5$ mm, $b = 3.5$ mm, $l = 20$ mm, $k_0 = 20$ N/m, $k_1 = 10$ N/m, $m = 0.01$ kg, and $I = 10^{-6}$ kg m². The entire structure is then 1.58 m long. (The numbers were chosen to represent those of a physical system that could be actually constructed.) The positions of each of the 80 masses as a function of time are shown in Fig. 5. It is possible to observe two distinct waves emanating from the origin in Fig. 5; the faster wave reaches the fixed mass at a normalized time of approximately 0.55, while the slower wave reaches the fixed mass at 1.0 (the time scale has been normalized by the time it takes for the slow wave to travel the bar length). A similar type of plot is presented in the work of Balk et al. (2001).

4.2. Comparison between a discrete and a continuous model

In this section, a discrete example described in Section 2.4 is compared with a continuous example from Section 2.2. The problem to be considered is the rigidly supported bar shown in Fig. 2. In the present example, the bar is homogeneous and there is no need to distinguish parameters with subscripts. From Appendix, the following constants for the continuous case are used:

$$A = 10.8, B = 1, C = -1, D = 0.02743. \quad (4.1)$$

Using Eqs. (2.6) and (2.33), the following equivalent discrete case constants are used: $a = 1$ m, $l = 1$ m, $k_0 = 9.8$ N/m, $k_1 = 1$ N/m, $m = 1$ kg, and $I = 0.02743$ kg m². To obtain the linear version of the discrete model that corresponds to the linear continuous model, it is necessary for $b \rightarrow 0$. A plot showing the normalized stress at the midpoint of each rod is given in Fig. 6. The two distinct waves are visible, noting that the faster wave is twice as fast as the slower wave since $\Gamma = 2$, see Eq. (A.1). With the exception of the oscillatory behavior of the underdamped discrete model, the two solutions cor-

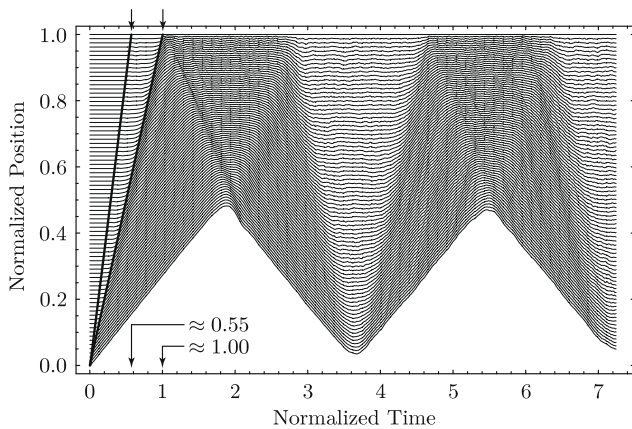


Fig. 5. The normalized axial positions for each of 80 discrete masses, connected as described by Fig. 4, are shown as functions of normalized time after a constant load is applied to the end $i = 1$. The end $i = 80$ is fixed for both axial deformation and rotation.

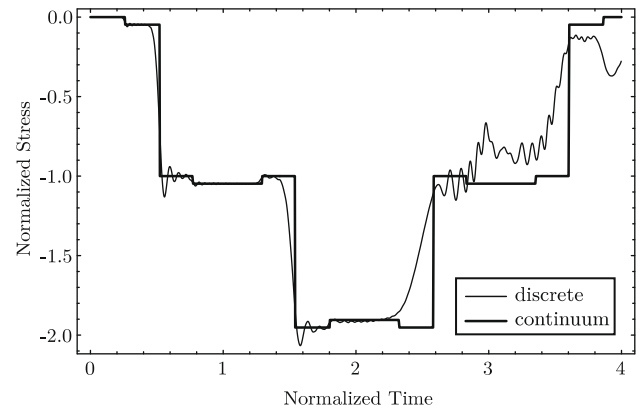


Fig. 6. Normalized stress at the midpoint of a discrete rod and a continuous rod is shown as a function of normalized time. Since stress at the midpoint is shown, the slow stress wave arrives at a normalized time of 0.5.

respond relatively well through the first three reflections of the stress waves, e.g., after a normalized time of two for the fast wave. After this point, the solutions begin to diverge. This is due to the fact that the boundary conditions between the two systems are fundamentally different. For the discrete model, a boundary is simply a mass at an end that is connected to only a single neighbor, while an interior mass is connected to two neighbors. In moving to the continuum, the interior structure of Fig. 4 is treated as a representative volume element and it is used to describe the behavior of the entire body. Hence, in Fig. 6, each time a wave reflects from a boundary, the results of the two models increasingly differ.

4.3. An impact problem with tuned micropolar bodies

The case to be considered here is an impact between two identical micropolar bodies – the flyer is of length $l = 1/3$ and the target is of length $1 - l = 2/3$, recalling Fig. 3. The model parameters have been chosen, or tuned, to ensure that the first occurrence of a net tensile stress appears at the interface between the bodies at $x = 1/3$. (In a non-polar material system, the initial net tensile stress will appear at $x = 2/3$, which is the middle of the target.) The following constants from Appendix are used:

$$A_1, A_2 = 10.8, B_1, B_2 = 1, C_1, C_2 = \pm 1, D_1, D_2 = 0.02743. \quad (4.2)$$

Fig. 7 is a shock wave position-versus-time, or x - t , diagram that shows the propagation of the stress waves (the faster wave as a

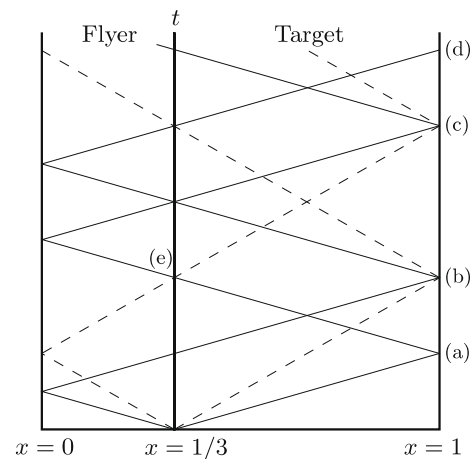


Fig. 7. The x - t diagram for the impact example with tuned parameters such that the initial net tensile stress occurs at point (e), the interface between flyer and target.

solid line and the slower wave as a dashed line) through both the flyer and target immediately after impact. The points in the figure are labeled to correspond with the points to be shown in Fig. 8. Point (e) denotes the time when a tensile stress state initiates at the interface between the flyer and the target. Only by assuming that the flyer and target remain attached can the stress waves continue to travel through the interface as they are shown to do in Fig. 7.

In a plate impact experiment, e.g., Antoun et al. (2003), the velocity of the free end of a target plate (at $x = 1$ for the example presented here) is measured as a function of time. The results of such an experiment are used to characterize the spall strength of the target material. Fig. 8 shows such an example for a micropolar target and flyer, characterized by Eq. (4.2). If the target and flyer were to separate when a tensile stress first appears at the interface (at point (e) in Fig. 7), Fig. 8 would only be valid up to the velocity jump at point (c). The results of Fig. 8 suggest that a micropolar body of the type described in Section 2.1 should possess two distinct jumps in velocity, at points (a) and (b), that are associated

with the distinct waves discussed in Section 4.1. The maximum velocity does not reach the initial velocity since the impact also produces rotational motion, in other words, the initial purely axial motion generates both axial deformation as shown in Fig. 8 as well as rotational motion. If there were no rotational motion, as in the case of a non-polar body, then $\dot{u}_2/\dot{v} = 1$ at its maximum.

In order to see the stress wave propagation for this example in greater detail, Fig. 9 shows four snapshots in time of the stress state in the flyer and the target. The arrival of the first stress wave at $x = 1$ (at point (a) in Figs. 7 and 8) is shown in the second of these figures. The initiation of a tensile stress state at the interface is seen to occur at the same time as the arrival of an initial compressive wave (the larger wave) and a reflected tensile wave (the smaller wave) at the free end, $x = 1$ (at Points (b) and (e) in Figs. 7 and 8). The fact that the stress waves begin as compressive waves and are reflected from the free surfaces $x = 0$ and $x = 1$ as tensile waves is apparent from Fig. 9 as well.

Although analytical solutions involving a finite number of unit step functions have been used thus far, it will be necessary to resort to numerical inversions of the Laplace transforms in Section 4.4. Therefore, one final example is shown in Fig. 10 comparing the numerical solution to the exact solution that was presented in Fig. 8. The numerical solution is found using the DAC algorithm with Lanczos' σ -factors with 512 terms and a tolerance equal to 10^{-4} , see Laverty and Gazonas (2006). As can be seen, the effect of the Gibbs phenomenon is minimal and so we can be confident in the results presented in the following section that make use of this numerical tool.

4.4. Impact with different materials

Since the plate impact test mentioned in the previous section is a common approach in the study of impact, results of the type presented in Fig. 8 will be considered in the examples to follow. The normalized velocities at the free end ($x = 1$) of a target impacted by a flyer for three different cases are shown in Fig. 11. The three cases include the following: a non-polar flyer and non-polar target (np-np), a micropolar flyer and micropolar target (mp-mp), and a non-polar flyer and micropolar target (np-mp). The micropolar material is described by Eq. (4.2), while the non-polar material is modeled with the following parameters:

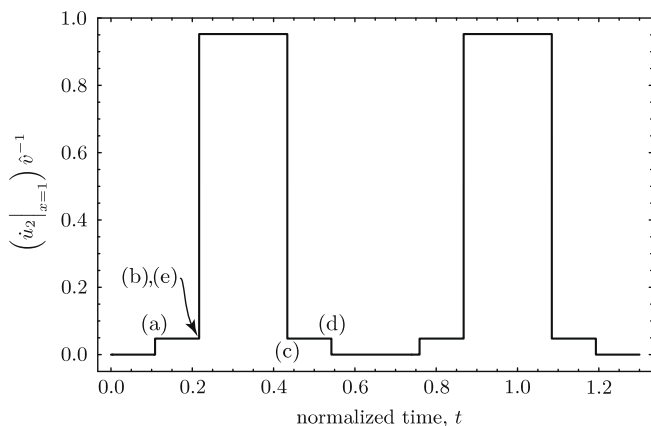


Fig. 8. The normalized velocity at the point $x = 1$ as a function of normalized time, assuming that the two bodies remain permanently attached from the moment of impact. The points (a)–(e) are the same as those shown in Fig. 7.

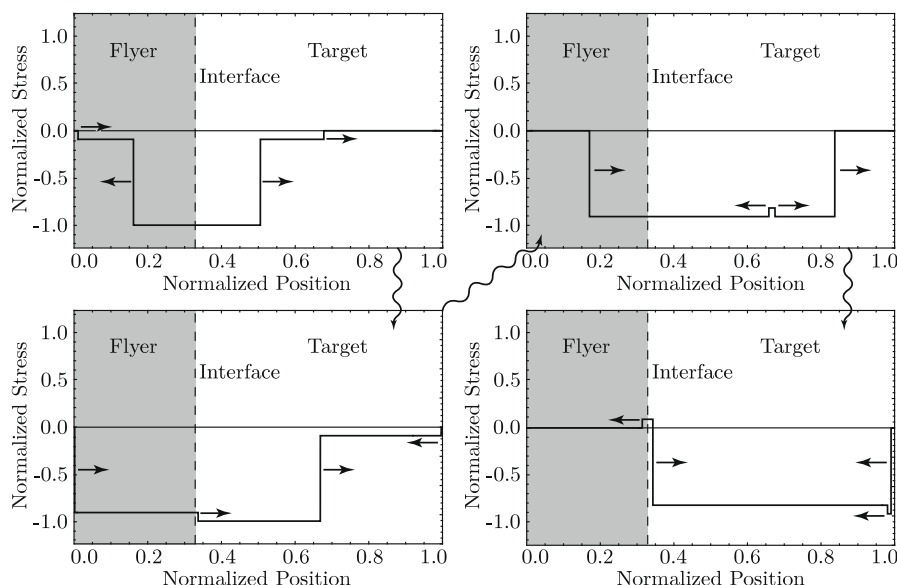


Fig. 9. The normalized stress state within the system at four different times, beginning with the top left figure and ending with the bottom right figure, is shown as a function of normalized position.

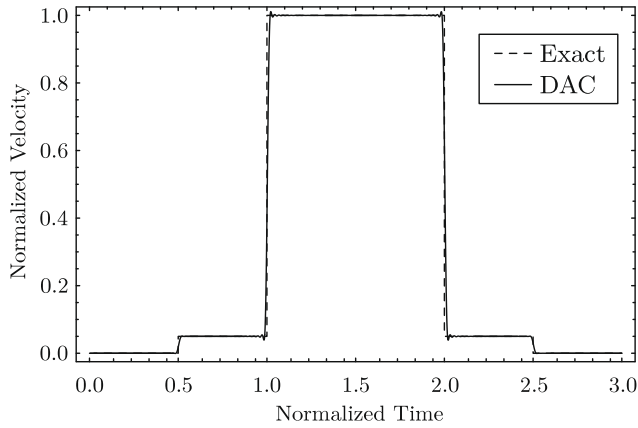


Fig. 10. To illustrate the effect of Gibbs phenomenon, the exact solution and the numerical solution from the DAC algorithm are plotted for the case shown in Fig. 8.

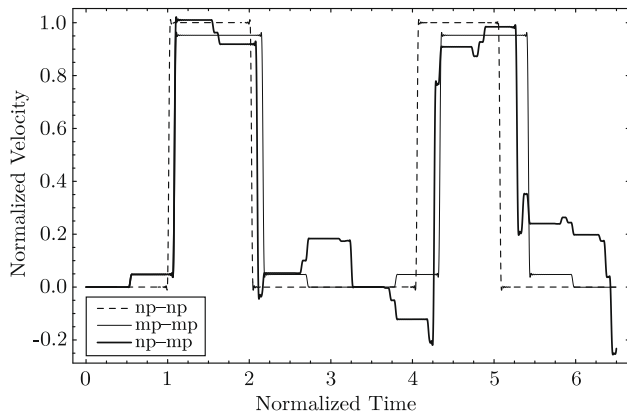


Fig. 11. Normalized velocity at the point $x = 1$ as a function of time as was shown in Fig. 8. In this figure, three examples are shown: non-polar flyer–non-polar target, micropolar flyer–micropolar target, and non-polar flyer–micropolar target.

$$A_1 = 10.8, B_1 = 10^6, C_1 = \pm 10^{-6}, D_1 = 0.02743 \times 10^6. \quad (4.3)$$

Compared with the micropolar case, the coupling constant C_1 is reduced by six orders of magnitude to reduce the coupling between axial deformation and rotation. In addition, the inertia and stiffness associated with rotation are increased by six order of magnitude. In terms of its ability to rotate, the body becomes extremely stiff (due to the increase in B_1) and insensitive to applied rotation deformations (due to the large microinertia that increases D_1).

According to Fig. 11, the initial response to impact for both micropolar targets is similar, exhibiting two distinct velocity jumps and identical wave speeds. This is due to the fact that the target materials are identical. The mismatch in material properties between flyer and target for the “np–mp” case leads to a more complex response, as waves are partially reflected and partially transmitted at the inter-

face between dissimilar materials. A detailed analysis of the reflection and transmission of waves across an interface with a mismatch in impedance is presented in Section 4.5.

4.5. Transmitted and reflected stress at the interface of a Two-Layer micropolar body

In addition to simply using the D'Alembert approach to solve the given boundary value problem, this approach also gives insight into the relationships between incident, transmitted, and reflected stress waves resulting from an impedance mismatch at the interface of two different materials described by different constitutive parameters. The interface is perpendicular to the direction of travel of the plane stress waves. Eringen (1999) considered harmonic plane waves traveling through micropolar bodies that reflect off of a free surface, while Ghosh et al. (2001) examined such waves transmitted across a boundary between two micropolar bodies.

For example, consider the case of two semi-infinite one-dimensional micropolar bars with an interface at $x = 0$, see Fig. 12(a) or (b). If the eight functions F_1 – F_8 are known, the behavior of each layer is completely described using Eqs. (3.1)–(3.3) and (3.4). If we only wish to solve for the reflection and transmission coefficients, it is not necessary to obtain all eight functions F_1 – F_8 . For example, since both bodies are semi-infinite, there is no need to consider boundaries at $\pm\infty$. Only the matching boundary conditions at $x = 0$ given by Eqs. (2.22)–(2.24) and (2.25) are used.

Based on the discussion in Section 4.1, there is a fast wave and a slow wave and each is capable of traveling towards the left and the right. Therefore, for each layer, there are four waves and four F -terms, F_1 – F_4 for Layer 1 and F_5 – F_8 for layer 2. For example, if the fast wave in layer 1 traveling to the right is the *incident* wave, then we are also only concerned with the *reflected* fast and slow waves and the *transmitted* fast and slow waves. In this particular case, F_2 corresponds to the incident fast wave, F_1 corresponds to the reflected fast wave, F_3 corresponds to the reflected slow wave, F_6 corresponds to the transmitted fast wave, and F_8 corresponds to the transmitted slow wave, see Fig. 12(a). The terms containing F_4 , F_5 , and F_7 may be neglected and we are left with four equations for five unknowns. Similar relationships hold for a slow incident stress wave, as shown see Fig. 12(b), and for incident waves traveling towards the left in layer 2.

For the case shown in Fig. 12(a) and recalling Eqs. (2.22)–(2.24) and (2.25), the four equations to be solved to find F_1 , F_3 , F_6 , and F_8 as functions of F_2 are

$$\frac{\mu_1}{\lambda_1} [\nabla F_1 + \nabla F_2] + \frac{\mu_2}{\lambda_1^+} \nabla_3 = \frac{\mu_3}{\lambda_2} \nabla F_6 + \frac{\mu_4}{\lambda_2^+} \nabla F_8, \quad (4.4)$$

$$\frac{1}{\lambda_1} [\nabla F_1 + \nabla F_2] + \frac{1}{\lambda_1^+} \nabla_3 = \frac{1}{\lambda_2} \nabla F_6 + \frac{1}{\lambda_2^+} \nabla F_8, \quad (4.5)$$

$$A_1 \{ \mu_1 [\nabla F_1 - \nabla F_2] + \mu_2 \nabla F_3 \} + C_1 [\nabla F_1 - \nabla F_2 + \nabla F_3] = A_2 [-\mu_3 \nabla F_6 - \mu_4 \nabla F_8] + C_2 [-\nabla F_6 - \nabla F_8], \quad (4.6)$$

$$C_1 \{ \mu_1 [\nabla F_1 - \nabla F_2] + \mu_2 \nabla F_3 \} + B_1 [\nabla F_1 - \nabla F_2 + \nabla F_3] = C_2 [-\mu_3 \nabla F_6 - \mu_4 \nabla F_8] + B_2 [-\nabla F_6 - \nabla F_8], \quad (4.7)$$

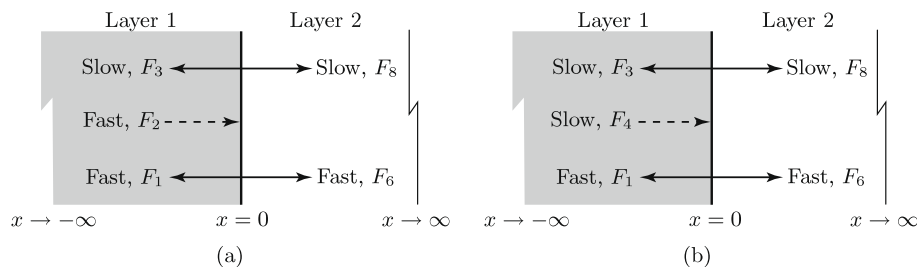


Fig. 12. Fig. 12(a) shows an incident fast plane wave traveling towards the right in layer 1 and the resulting transmitted and reflected plane waves. Fig. 12(b) shows the same for a slow incident wave.

where $\nabla F_1 \equiv \nabla F_1(t/\lambda_1^-)$, $\nabla F_2 \equiv \nabla F_2(t/\lambda_1^-)$, $\nabla F_3 \equiv \nabla F_3(t/\lambda_1^+)$, $\nabla F_6 \equiv \nabla F_6(t/\lambda_2^-)$, and $\nabla F_8 \equiv \nabla F_8(t/\lambda_2^+)$ since the interface is taken to be at $x = 0$. Eqs. (4.4) and (4.5) are taken from Eqs. (2.22) and (2.23), where the gradient appears after taking the derivative with respect to time from Eqs. (2.22) and (2.23) and substituting Eqs. (3.1)–(3.3) and (3.4). Eqs. (4.6) and (4.7) come directly from Eqs. (2.24) and (2.25).

Eqs. (4.4)–(4.6) and (4.7) are used to solve for ∇F_1 , ∇F_3 , ∇F_6 , and ∇F_8 in terms of ∇F_2 , λ_1^\pm , λ_2^\pm , $\mu_1 - \mu_4$, $A_{1,2}$, $B_{1,2}$, and $C_{1,2}$. The ratio of the fast reflected (force) stress wave to the fast incident (force) stress wave is

$$\left(\frac{\nabla F_1}{\nabla F_2}\right) \frac{A_1 \mu_1 + C_1}{A_1 \mu_1 + C_1} \rightarrow \frac{\nabla F_1}{\nabla F_2}, \quad (4.8)$$

according to Eq. (2.8). The ratios for the slow reflected wave to the incident wave, the fast transmitted wave to the incident wave, and the slow transmitted wave to the incident wave are

$$\left(\frac{\nabla F_3}{\nabla F_2}\right) \frac{A_1 \mu_2 + C_1}{A_1 \mu_1 + C_1}, \quad \left(\frac{\nabla F_6}{\nabla F_2}\right) \frac{A_2 \mu_3 + C_2}{A_1 \mu_1 + C_1}, \quad \left(\frac{\nabla F_8}{\nabla F_2}\right) \frac{A_2 \mu_4 + C_2}{A_1 \mu_1 + C_1}, \quad (4.9)$$

respectively. For the case of the same four ratios, but now with respect to the incident slow wave, one would make use of the following four quantities:

$$\left(\frac{\nabla F_1}{\nabla F_4}\right) \frac{A_1 \mu_1 + C_1}{A_1 \mu_2 + C_1}, \quad \frac{\nabla F_3}{\nabla F_4}, \quad \left(\frac{\nabla F_6}{\nabla F_4}\right) \frac{A_2 \mu_3 + C_2}{A_1 \mu_2 + C_1}, \quad \left(\frac{\nabla F_8}{\nabla F_4}\right) \frac{A_2 \mu_4 + C_2}{A_1 \mu_2 + C_1}, \quad (4.10)$$

since F_4 corresponds to the incident slow wave.

As an example, consider two bars with a normalized (force) stress applied at \hat{T} at $x = 0$ and rigidly fixed at $x = 1$, see Fig. 2. One bar is non-polar, described by the material properties of Eq. (4.3), and the other bar consists of two layers. The bar is non-polar between $0 \leq x \leq 1/2$ and micropolar between $1/2 \leq x \leq 1$. For the two-layer bar, the slow stress wave is the incident wave transmitted through the non-polar body that reaches the interface between the layers. By considering the third and fourth quantities in Eq. (4.10), it is possible to find material parameters that will reduce the stress transmitted across the interface. By equating the stress corresponding to the fast and slow transmitted waves, it is possible to obtain the following parameters:

$$A_2 = 10.8, B_2 = 10^2, C_2 = \pm 27.57, D_2 = 0.02743 \times 10^2. \quad (4.11)$$

By examining the transmission and reflection coefficients obtained via the D'Alembert method, it is discovered that the ratio of the transmitted fast and slow waves to the incident wave is 0.442; the ratio of the reflected slow wave to the incident wave is 0.116. These results are shown in Fig. 13 for a homogeneous bar and a two-layer bar at the positions indicated to the left of the center

(a) and to the right of the center (b) of each bar. The results shown in Fig. 13 are obtained by solving the mixed boundary-initial value problem via the Laplace transform approach and using the DAC algorithm. By observation, the results of both approaches are the same, thus confirming the solution techniques employed. That is, the reflected (dashed) stress shown in Fig. 13(a) has a magnitude of 0.116; both transmitted (dashed) waves in Fig. 13(b) have magnitudes of 0.442.

5. Summary

A one-dimensional model of a linear, anisotropic, micropolar body subjected to transient loading associated with impact has been presented. In particular, this model has been solved for the case of a two-layer bar subjected to a known stress at one end and rigidly fixed at the other end. Either one or both layers may be considered as micropolar bodies, each of which is described by four model parameters. The model has also been solved for an impact problem consisting of a micropolar projectile and a micropolar target. These results may be used to model high strain rate experiments, such as Kolsky bar tests and plate impact tests, or to give insight into how such materials would behave as armors subjected to blast and/or ballistic impact. A discrete model has also been solved and the model parameters used in the micropolar continuum model have been related to the properties of the discrete model, which are physically more understandable.

By analyzing the solutions to the governing PDEs, we have been able to choose model parameters to control the reflection and transmission coefficients resulting from an impedance mismatch at the interface of two different materials. This allows us to control the transmission of stress that results from blast or impact. For the case of impact, we have also been able to control where the tensile stress wave first appears. This is helpful since materials often fail in tension as a result of the combination of reflected, initially compressive, stress waves caused by impact. These preliminary results suggest the possibility of designing an optimal system that will best withstand the high strain rate loads it will be subjected to in service. This sort of optimization has been done for the case of multi-layered elastic strips by Velo and Gazonas (2003).

The analysis presented herein has been limited to linear behavior, i.e., requiring small displacements and assuming linear relations between stress and strain. In addition, it has been necessary to assume a periodic microstructure, an assumption that may be valid in the case of an engineered structure but less realistic for the case of a pulverized ceramic. By adding heterogeneity to the discrete model presented in Section 2.4, a homogenization analysis approach may be used to examine the effects of a less regular structure, although a fully random structure necessitates a different approach, see Ostojca-Starzewski and Trębicki (1999), Ostojca-Starzewski and Trębicki (2003). Even with these approxi-

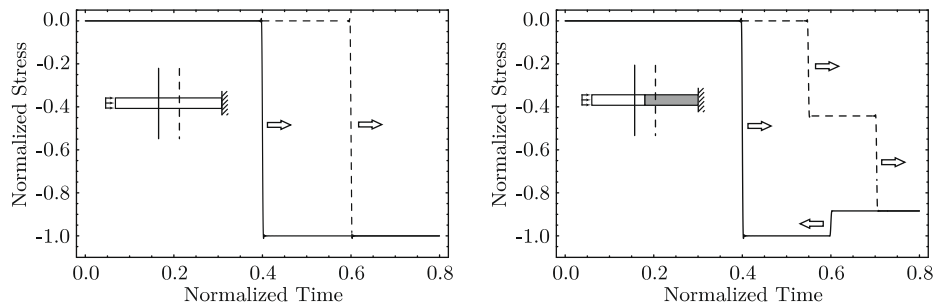


Fig. 13. Normalized stress waves at $x = 0.4$ and $x = 0.6$ are shown for a uniform, non-polar bar and a two-layer bar (the first layer is non-polar and the second layer is micropolar). The solid lines indicate the stress state at $x = 0.4$, while the dashed lines indicate the stress state at $x = 0.6$. The arrows indicate the directions the waves are traveling.

mations, the current work serves as a benchmark for moving to higher dimensions and more complex constitutive relations, where it becomes more difficult to relate micropolar constitutive parameters to physical systems. In this way, the results presented here will guide the development of more advanced models better capable of describing the response of multi-scale materials to impact and blast conditions.

Acknowledgment

The first author acknowledges that this research was supported in part by an appointment to the U.S. Army Research Laboratory Postdoctoral Fellowship Program administered by the Oak Ridge Associated Universities through a contract with the U.S. Army Research Laboratory.

Appendix. Choosing constants for the micropolar model

In this appendix, the parameters given in Eqs. (4.1) and (4.2) will be calculated. The goal here is to determine model parameters that ensure the following:

- The faster wave speed will be twice the magnitude of the slower wave speed ($\Gamma = 2$, see the following justification for this requirement), and
- the stress corresponding to the slower wave speed will be larger than the stress corresponding to the faster wave speed for the case with no applied couple stress.

In a traditional plate impact test involving non-polar materials, the target material will fail under a tensile load generated at the middle of the target specimen, assuming that the target is twice the thickness of the flyer and both materials are identical. As a demonstration of the nature of the micropolar material as described herein, we have decided to present an example where the initial tensile stress appears at the target-flyer interface, rather than within the target. Since the typical target-length-to-flyer-length ratio equals two, it will be necessary to require $\Gamma = 2$. There are no additional limitations imposed on the solution under these requirements. Since the two bodies are identical, there is no need to specify different properties through the use of subscripts. The ratio of the fast wave speed to the slow wave speed, Γ , mentioned in the first of the two requirements is defined as

$$\Gamma = \frac{\text{Fast Wave Speed}}{\text{Slow Wave Speed}} = \frac{1/\lambda^-}{1/\lambda^+} > 1, \quad (\text{A.1})$$

since $\lambda^+ > \lambda^-$, see Section 3.1. Based on Eqs. (3.6)–(3.9) and (3.10) and the requirement on Γ in Eq. (A.1), it follows that the model parameter C equals

$$C = \pm \frac{1}{1 + \Gamma^2} \sqrt{AB(1 + \Gamma^4) - B^2 D^{-1} \Gamma^2 - A^2 D \Gamma^2}. \quad (\text{A.2})$$

Based on the first of Eq. (2.8) and the solutions to Eqs. (2.14) and (2.15) for identical flyer and target materials, the ratios of the stresses corresponding to the fast and slow waves are given by

$$\Delta = \frac{T_{\text{fast}}}{T_{\text{slow}}} = -\left(\frac{\mu_1 A + C}{\mu_2 A + C}\right) \left(\frac{\mu_2 C + B}{\mu_1 C + B}\right) = -\frac{\mu_1}{\mu_2}, \quad \frac{M_{\text{fast}}}{M_{\text{slow}}} = 1, \quad (\text{A.3})$$

for the case with no applied couple stress. Next, the ratios of the particle speeds of the two axial waves with no applied couple stress are

$$\frac{\text{Fast-Wave Translational Particle Speed}}{\text{Slow-Wave Translational Particle Speed}} = -\frac{\mu_1}{\mu_2} \left(\frac{\lambda^+}{\lambda^-}\right) = \Delta \Gamma, \quad (\text{A.4})$$

and

$$\frac{\text{Fast-Wave Rotational Particle Speed}}{\text{Slow-Wave Rotational Particle Speed}} = \frac{\lambda^+}{\lambda^-} = \Gamma. \quad (\text{A.5})$$

If there is only a single wave present, as in the classical, non-polar case, then $\Delta \rightarrow 0$ or $\Delta \rightarrow \infty$. By applying Eqs. (3.5) and (A.2) to Eq. (A.3) and solving for D , it follows that

$$D = \frac{B}{A} \left(\frac{1 + \Gamma^2 \Delta}{\Gamma^2 + \Delta} \right). \quad (\text{A.6})$$

Based on the inequalities in Eqs. (2.9) and (A.1), it follows that C equals zero only when $\Delta \rightarrow 0$ or $\Delta \rightarrow \infty$, i.e., the condition of a single wave. In the limit, if $\Gamma \rightarrow \infty$, C equals $\pm\sqrt{AB}$ based on applying Eq. (A.4) to (A.2); this is a violation of the last inequality in Eq. (2.9). Therefore, Γ must be finite and greater than one. Since $A, B, \Gamma, \Delta \geq 0$, C must be real. In conclusion then, to ensure that $C \neq 0$, it is necessary for $0 < \Delta < \infty$ and $1 < \Gamma < \infty$. Now we may consider actual numbers for our model. In addition to requiring $\Gamma = 2$, we will choose $\Delta = 0.1$ so that $T_{\text{slow}} > T_{\text{fast}}$. Making use of Eqs. (A.2) and (A.6), it follows that

$$C = \pm \left(\frac{\sqrt{30}}{18} \right) \sqrt{AB} = \pm 0.3043 \sqrt{AB}, \quad D = \left(\frac{8}{27} \right) \frac{B}{A} = (0.2963) \frac{B}{A}. \quad (\text{A.7})$$

The values of A and B were chosen to make C equal ± 1 , i.e., $\sqrt{AB} = 18/\sqrt{30}$, such that

$$A = 18^2/30 = 10.8, \quad B = 1, \quad C = \pm 1, \quad D = 20/729 = 0.02743. \quad (\text{A.8})$$

These model parameters are rewritten as Eqs. (4.1) and (4.2); there are no units associated with these parameters due to the non-dimensional formulation of Section 2.1.

References

- Antoun, T., Seaman, L., Curran, D., Kanel, G., Razorenov, S., Utkin, A., 2003. Spall Fracture. Springer-Verlag, New York.
- Balk, A., Cherkov, A., Slepyan, L., 2001. Dynamics of chains with non-monotone stress-strain relations. II. Nonlinear waves and waves of phase transmission. *Journal of the Mechanics and Physics of Solids* 49, 149–171.
- Crump, K., 1976. Numerical inversion of Laplace transforms using a Fourier series approximation. *Journal of the ACM* 23 (1), 89–96.
- Eringen, A., 1999. Microcontinuum Field Theories. I. Foundations and Solids. Springer, New York.
- Gazonas, G., Allen, D., 2003. Stress waves and cohesive failure in a finite strip subjected to transient loading. In: *Proceedings of the Ninth International Conference on the Mechanical Behaviour of Materials*, Geneva, Switzerland.
- Ghosh, N., Nath, S., Debnath, L., 2001. Propagation of waves in micropolar solid-solid semispaces in the presence of a compressional wave source in the upper solid substratum. *Mathematical and Computer Modelling* 34, 557–563.
- Goldsmith, W., 1999. Impact. Springer, New York.
- Jiang, W., Wang, T., Jones, W., 1991. Forced vibration of coupled extensional-torsional systems. *Journal of Engineering Mechanics* 117 (5), 1171–1190.
- Krishnaswamy, S., Batra, R., 1998. On extensional oscillations and waves in elastic rods. *Mathematics and Mechanics of Solids* 3, 277–295.
- Lavery, R., Gazonas, G., 2006. An improvement to the Fourier series method for inversion of Laplace transforms applied to elastic and viscoelastic waves. *International Journal of Computational Methods* 3 (1), 57–69.
- Lisina, S., Potapov, A., Nesterenko, V., 2001. A nonlinear granular medium with particle rotation: a one-dimensional model. *Acoustical Physics* 47 (5), 685–693.
- Martin, P., Berger, J., 2002. On mechanical waves along aluminum conductor steel reinforced (ACSR) power lines. *Journal of Applied Mechanics* 69, 740–748.
- Mindlin, R., 1964. Micro-structure in linear elasticity. *Archive for Rational Mechanics and Analysis* 16, 51–78.
- Ostoja-Starzewski, M., 2002. Lattice models in micromechanics. *Applied Mechanics Reviews* 55 (1), 35–60.
- Ostoja-Starzewski, M., Trębicki, J., 1999. On the growth and decay of acceleration waves in random media. *Proceedings of the Royal Society of London A* 455, 2577–2614.
- Ostoja-Starzewski, M., Trębicki, J., 2003. On the distance to blow-up of acceleration waves in random media. *Continuum Mechanics and Thermodynamics* 15, 21–32.
- Pastrone, F., 2005. Wave propagation in microstructured solids. *Mathematics and Mechanics of Solids* 10, 349–357.

- Pavlov, I., Potapov, A., Maugin, G., 2006. A 2D granular medium with rotating particles. *International Journal of Solids and Structures* 43 (20), 6194–6207.
- Plona, T., 1980. Observations of a second bulk compressional wave in a porous medium at ultrasonic frequencies. *Applied Physics Letters* 36 (4), 259–261.
- Porubov, A., Pastrone, F., 2004. Non-linear bell-shaped and kink-shaped strain waves in microstructured solids. *Non-Linear Mechanics* 39, 1289–1299.
- Puglisi, G., Truskinovsky, L., 2000. Mechanics of a discrete chain with bi-stable elements. *Journal of the Mechanics and Physics of Solids* 48, 1–27.
- Raoof, M., Huang, Y., Pithia, K., 1994. Response of axially preloaded spiral strands to impact loading. *Computers and Structures* 51 (2), 125–135.
- Samras, R., Skop, R., Milburn, D., 1974. An analysis of coupled extensional-torsional oscillations in wire rope. *Journal of Engineering for Industry* 96, 1130–1135.
- Schanz, M., Cheng, A., 2000. Transient wave propagation in a one-dimensional poroelastic column. *Acta Mechanica* 145, 1–18.
- Schanz, M., Cheng, A., 2001. Dynamic analysis of a one-dimensional poroviscoelastic column. *Journal of Applied Mechanics* 68, 192–198.
- Shahsavari, H., Ostoj-Starzewski, M., 2005. On elastic and viscoelastic helices. *Philosophical Magazine* 85, 4213–4230.
- Slepyan, L., Cherkaev, A., Cherkaev, E., 2005. Transition waves in bistable structures. II. Analytical solution: wave speed and energy dissipation. *Journal of the Mechanics and Physics of Solids* 53 (2), 407–436.
- Velo, A., Gazonas, G., 2003. Optimal design of a two-layered elastic strip subjected to transient loading. *International Journal of Solids and Structures* 40, 6417–6428.
- YuFeng, X., DeChao, Z., 1998. Analytical solutions of impact problems of rod structures with springs. *Computer Methods in Applied Mechanics and Engineering* 160, 315–323.

NO. OF
COPIES ORGANIZATION

1 DEFENSE TECHNICAL
(PDF INFORMATION CTR
only) DTIC OCA
8725 JOHN J KINGMAN RD
STE 0944
FORT BELVOIR VA 22060-6218

1 DIRECTOR
US ARMY RESEARCH LAB
IMNE ALC HR
2800 POWDER MILL RD
ADELPHI MD 20783-1197

1 DIRECTOR
US ARMY RESEARCH LAB
AMSRD ARL CI OK TL
2800 POWDER MILL RD
ADELPHI MD 20783-1197

1 DIRECTOR
US ARMY RESEARCH LAB
AMSRD ARL CI OK PE
2800 POWDER MILL RD
ADELPHI MD 20783-1197

ABERDEEN PROVING GROUND

1 DIR USARL
AMSRD ARL CI OK TP (BLDG 4600)

<u>NO. OF COPIES</u>	<u>ORGANIZATION</u>
1 (CD only)	DPTY ASSIST SCT FOR R&T SARD TT ASA (ACT) J PARMENTOLA THE PENTAGON RM 3E479 WASHINGTON DC 20310-1714
1	PRIN DPTY FOR TCHNLGY HQ US ARMY MATCOM AMCDCGR R PRICE 9301 CHAPEK RD FT BELVOIR VA 22060-5527
3	AIR FORCE ARMAMENT LAB AFATL DLJW W COOK D BELK J FOSTER EGLIN AFB FL 32542
2	DARPA L CHRISTODOULOU W COBLENZ 3701 N FAIRFAX DR ARLINGTON VA 22203-1714
1	DIRECTOR US ARMY ARDEC AMSRD AAR AEE W E BAKER BLDG 3022 PICATINNY ARSENAL NJ 07806-5000
2	US ARMY TARDEC AMSTRA TR R MS 263 K BISHNOI D TEMPLETON MS 263 WARREN MI 48397-5000
1	COMMANDER US ARMY RSRCH OFC AMSRD ARL RO EN B LAMATTINA PO BOX 12211 RESEARCH TRIANGLE PARK NC 27709-2211

<u>NO. OF COPIES</u>	<u>ORGANIZATION</u>
1	COMMANDER US ARMY RSRCH OFC AMSRD ARL RO MM J LAVERY PO BOX 12211 RESEARCH TRIANGLE PARK NC 27709-2211
1	COMMANDER US ARMY RSRCH OFC AMSRD ARL RO EM D STEPP PO BOX 12211 RESEARCH TRIANGLE PARK NC 27709-2211
5	NAVAL RESEARCH LAB E R FRANCHI CODE 7100 M H ORR CODE 7120 J A BUCARO CODE 7130 J S PERKINS CODE 7140 S A CHIN BING CODE 7180 4555 OVERLOOK AVE SW WASHINGTON DC 20375
1	DTRA M GILTRUD 8725 JOHN J KINGMAN RD FORT BELVOIR VA 22060
1	ERDC US ARMY CORPS OF ENGINEERS USACEGSL P PAPADOS 7701 TELEGRAPH RD ALEXANDRIA VA 22315
1	CLEMSON UNIV DEPT MECH ENGINEERS M GRUJICIC 241 ENGRG INNOVATION BLDG CLEMSON SC 29634-0921
1	UNIV OF CALIFORNIA CTR OF EXCELLENCE FOR ADV MATLS S NEMAT NASSER SAN DIEGO CA 92093-0416

NO. OF
COPIES ORGANIZATION

5 DIRECTOR
LANL
P MAUDLIN
R GRAY
W R THISSELL
A ZUREK
F ADDESSIO
PO BOX 1663
LOS ALAMOS NM 87545

7 DIRECTOR
SANDIA NATL LABS
J BISHOP MS 0346
E S HERTEL JR MS 0382
W REINHART MS 1181
T VOGLER MS 1181
L CHHABILDAS MS 1811
M FURNISH MS 1168
M KIPP MS 0378
PO BOX 5800
ALBUQUERQUE NM 87185-0307

1 DIRECTOR
LLNL
M J MURPHY
PO BOX 808
LIVERMORE CA 94550

3 CALTECH
M ORTIZ MS 105 50
G RAVICHANDRAN
T J AHRENS MS 252 21
1201 E CALIFORNIA BLVD
PASADENA CA 91125

5 SOUTHWEST RSRCH INST
C ANDERSON
K DANNEMANN
T HOLMQUIST
G JOHNSON
J WALKER
PO DRAWER 28510
SAN ANTONIO TX 78284

1 TEXAS A&M UNIV
DEPT OF MATHEMATICS
J WALTON
COLLEGE STATION TX 77843

NO. OF
COPIES ORGANIZATION

2 SRI INTERNATIONAL
D CURRAN
D SHOCKEY
333 RAVENSWOOD AVE
MENLO PARK CA 94025

1 VIRGINIA POLYTECHNIC INST
COLLEGE OF ENGRG
R BATRA
BLACKSBURG VA 24061-0219

8 UNIV OF NEBRASKA
DEPT OF ENGRG MECH
D ALLEN
F BOBARU
Y DZENIS
G GOGOS
M NEGAHBAN
R FENG
J TURNER
Z ZHANG
LINCOLN NE 68588

1 JOHNS HOPKINS UNIV
DEPT OF MECH ENGRG
K T RAMESH
LATROBE 122
BALTIMORE MD 21218

1 WORCESTER POLYTECHNIC INST
MATHEMATICAL SCI
K LURIE
WORCESTER MA 01609

4 UNIV OF UTAH
DEPT OF MATH
A CHERKAEV
E CHERKAEV
E S FOLIAS
R BRANNON
SALT LAKE CITY UT 84112

1 PENN STATE UNIV
DEPT OF ENGRG SCI & MECH
F COSTANZO
UNIVERSITY PARK PA 168023

3 UNIV OF DELAWARE
DEPT OF MECH ENGRG
T BUCHANAN
T W CHOU
M SANTARE
126 SPENCER LAB
NEWARK DE 19716

NO. OF
COPIES ORGANIZATION

1 UNIV OF DELAWARE
CTR FOR COMPST MATRLS
J GILLESPIE
NEWARK DE 19716

1 COMPUTATIONAL MECH
CONSULTANTS
J A ZUKAS
PO BOX 11314
BALTIMORE MD 21239-0314

1 LOUISIANA STATE UNIV
R LIPTON
304 LOCKETT HALL
BATON ROUGE LA 70803-4918

2 INST OF ADVANCED TECH
UNIV OF TX AUSTIN
S BLESS
H FAIR
3925 W BRAKER LN STE 400
AUSTIN TX 78759-5316

1 APPLIED RSCH ASSOCIATES
D E GRADY
4300 SAN MATEO BLVD NE
STE A220
ALBUQUERQUE NM 87110

1 INTERNATIONAL RSRCH
ASSOC INC
D L ORPHAL
4450 BLACK AVE
PLEASANTON CA 94566

1 AKT MISSION RSRCH CORP
M EL RAHEB
23052 ALCALDE DR
LAGUNA HILLS CA 92653

1 UNIV OF ILLINOIS
DEPT OF MECHL SCI & ENGRG
A F VAKAKIS
1206 W GREEN ST MC 244
URBANA CHAMPAIGN IL 61801

1 UNIV OF ILLINOIS
ARSPC ENGRG
J LAMBROS
104 S WRIGHT ST MC 236
URBANA CHAMPAIGN IL 61801

NO. OF
COPIES ORGANIZATION

2 WASHINGTON ST UNIV
INST OF SHOCK PHYSICS
Y M GUPTA
J ASAY
PULLMAN WA 99164-2814

1 ARIZONA STATE UNIV
MECHCL & ARSPC ENGRG
D KRAJCINOVIC
TEMPE AZ 85287-6106

1 NORTHWESTERN UNIV
DEPT OF CIVIL & ENVIRON ENGRG
Z BAZANT
2145 SHERIDAN RD A135
EVANSTON IL 60208-3109

1 UNIV OF DAYTON
RSRCH INST
N S BRAR
300 COLLEGE PARK
MS SPC 1911
DAYTON OH 45469

2 TEXAS A&M UNIV
DEPT OF GEOPHYSICS MS 3115
F CHESTER
T GANGI
COLLEGE STATION TX 778431

1 UNIV OF SAN DIEGO
DEPT OF MATH & CMPTR SCI
A VELO
5998 ALCALA PARK
SAN DIEGO CA 92110

1 NATIONAL INST OF
STANDARDS & TECHLGY
BLDG & FIRE RSRCH LAB
J MAIN
100 BUREAU DR MS 8611
GAITHERSBURG MD 20899-8611

1 MIT
DEPT ARNTCS ASTRNTCS
R RADOVITZKY
77 MASSACHUSETTS AVE
CAMBRIDGE MA 02139

NO. OF
COPIES ORGANIZATION

1 MIT
DEPT MATLS SCI ENGRG
E THOMAS
77 MASSACHUSETTS AVE
CAMBRIDGE MA 02139

2 MATERIALS SCI CORP
A CAIAZZO
R LAVERTY
181 GIBRALTAR RD
HORSHAM PA 19044

2 DIR USARL
AMSRD ARL D
C CHABALOWSKI
V WEISS
2800 POWDER MILL RD
ADELPHI MD 20783-1197

ABERDEEN PROVING GROUND

81 DIR USARL
AMSRD ARL WM
S KARNA
J MCCAULEY
P PLOSTINS
J SMITH
T WRIGHT
AMSRD ARL WM B
J NEWILL
M ZOLTOSKI
AMSRD ARL WM BA
D LYON
AMSRD ARL WM BC
P WEINACHT
AMSRD ARL WM BD
P CONROY
B FORCH
R PESCE RODRIGUEZ
B RICE
AMSRD ARL WM BF
W OBERLE
AMSRD ARL WM M
R DOWDING
S MCKNIGHT
AMSRD ARL WM MA
J ANDZELM
R JENSEN
A RAWLETT
M VANLANDINGHAM
E WETZEL
AMSRD ARL WM MB
M BERMAN
T BOGETTI

NO. OF
COPIES ORGANIZATION

M CHOWDHURY
W DE ROSSET
W DRYSDALE
A FRYDMAN
D HOPKINS
L KECSKES
T H LI
S MATHAUDHU
M MINNICINO
B POWERS
J TZENG
AMSRD ARL WM MC
R BOSSOLI
S CORNELISON
M MAHER
W SPURGEON
AMSRD ARL WM MD
J ADAMS
B CHEESEMAN
E CHIN
K CHO
B DOOLEY
C FOUNTZOULAS
G GAZONAS
J LASALVIA
P PATEL
C RANDOW
J SANDS
B SCOTT
C F YEN
AMSRD ARL WM SG
T ROSENBERGER
AMSRD ARL WM T
P BAKER
M BURKINS
AMSRD ARL WM TA
S SCHOENFELD
AMSRD ARL WM TB
N ELDREDGE
J STARKENBERG
AMSRD ARL WM TC
T BJERKE
T FARRAND
K KIMSEY
M FERREN COKER
D SCHEFFLER
S SCHRAML
S SEGLETES
AMSRD ARL WM TD
S BILYK
D CASEM
J CLAYTON
D DANDEKAR
N GNIAZDOWSKI

NO. OF
COPIES ORGANIZATION

M GREENFIELD
R KRAFT
B LOVE
M RAFTENBERG
E RAPACKI
M SCHEIDLER
T WEERASOORIYA
AMSRD ARL WM TE
J POWELL
B RINGERS
G THOMSON
AMSRD ARL WM UV
S WILKERSON
AMSRD ARL VT RP
J BORNSTEIN

INTENTIONALLY LEFT BLANK.